

Experimental Study on Composite Action in Reinforced Concrete–Filled Steel-Tube Shaft Foundations

Hadi Kenarangi, S.M.ASCE¹; and Michel Bruneau, F.ASCE²

Abstract: A single enlarged shaft foundation is often used to support bridge columns. In some conditions, it is constructed with a permanent steel casing, which is typically ignored in calculating the structural resistance of the shaft. This study investigated the contribution of this steel casing to the structural resistance and seismic response of single shaft foundations. The composite action between the steel casing and the interior reinforced concrete shaft was investigated. A series of six cyclic large-scale tests were conducted on cantilevering shafts of 50.8- and 76.2-cm diameters with heights of 5.2 and 7.6 m, respectively, with reinforced concrete columns at their top. Different interface conditions were applied to the specimens, which included the natural bond, grease, bentonite slurry, and use of shear mechanisms. In addition to the different interface conditions, the effects of the diameter-to-thickness ratio ($D:t$) and applied axial load were also considered. The composite behavior of the tested specimens and the plastic hinge development under large deformations were investigated and compared to results from plastic moment calculations. DOI: 10.1061/(ASCE)BE.1943-5592.0001407. © 2019 American Society of Civil Engineers.

Author keywords: Reinforced concrete–filled steel tubes; Composite construction; Drilled shafts; Cyclic testing; Flexural strength; Columns; Shear transferring mechanism; Axial loading.

Introduction and Background

Bridges are often constructed with a single enlarged shaft foundation supporting a column. In many cases, the shaft foundation is constructed with a permanent steel casing. Although this is done mostly for support of the drilled shaft excavation, these casings, which are typically steel tubes (joined by welding if necessary), may be considered a structural element of the completed drilled shaft, effectively creating a composite structural member. Bridge designers would like to account for the added structural resistance of the steel casing, but there are limited research data as to when the steel casing and concrete inner core act as a composite section in these members. Therefore, the steel casing is typically ignored in design when calculating the structural resistance of the shaft. This is reflected in a report published by the Federal Highway Administration (FHWA) (Brown et al. 2010), which recommends designing the shaft as a reinforced concrete beam column (reinforcement cages are typically present in the shaft). Article 5.13.4.5.2 of AASHTO LRFD Bridge Design Specifications (AASHTO BDS) (AASHTO 2014b) suggests that the steel casing may be considered in computing structural strength but does not provide any specifications on how this can be accomplished. Most of the state Departments of Transportation (DOTs; i.e., 35 states) follow AASHTO BDS (AASHTO 2014b) for including the resistance of the casing in design of the shafts. Of

the remaining states that do not follow AASHTO, four of them allow the inclusion of the resistance of the steel casing in design of the shaft [i.e., California (Caltrans 2010), Missouri (Missouri Dept. of Transportation 2011), Oregon (Oregon Dept. of Transportation 2013), and Washington (WDOT 2016)]. Seven do not allow or advise not to use the steel casing resistance in the design [i.e., Florida (FDOT 2000), Kansas (KDOT 2013), Kentucky (Mark Hite, personal communication, 2013), Nevada (NDOT 2008), North Carolina (Brian Hanks, personal communication, 2013), South Carolina (SCDOT 2008), and Virginia (John M. Hall, personal communication, 2013)], and the rest do not have any specifications regarding the inclusion of the steel casing in design (i.e., Massachusetts, Illinois, Oklahoma, and New Mexico).

The encased reinforced concrete shaft foundations are generally referred as reinforced concrete–filled steel tube (RCFST) shafts. Developing the strength of the steel casing in drilled shafts implies that the shaft will ultimately behave as a fully composite RCFST, or a noncomposite one, but adding strength in both cases. The noncomposite case refers to a state where the strain distributions in the steel casing and the reinforced concrete core are independent of each other when subjected to bending. In most cases, the flexural strength of the noncomposite RCFST is on the order of 10%–20% less than that of the composite case (Bruneau et al. 2018). The strength difference between noncomposite and composite cases is attributed to the differences in the positions of the neutral axes. For a noncomposite RCFST section under bending and zero axial load, the positions of neutral axes on the steel tube and the reinforced concrete core will be independent of each other and not coincide. In fact, in zero axial load conditions, the neutral axis of the steel tube is at the center of the cross section, whereas for the reinforced concrete core, it is toward the side of the cross section that is under compression. When full composite strength is developed, the neutral axes of the steel tube and the reinforced concrete core cross sections will be the same. The shifting of neutral axes of

¹Graduate Research Assistant, Dept. of Civil Structural and Environmental Engineering, Univ. at Buffalo, Buffalo, NY 14260 (corresponding author). ORCID: <https://orcid.org/0000-0002-8750-7722>. Email: hadikena@buffalo.edu

²Professor, Dept. of Civil Structural and Environmental Engineering, Univ. at Buffalo, Buffalo, NY 14260. Email: bruneau@buffalo.edu

Note. This manuscript was submitted on March 7, 2018; approved on December 12, 2018; published online on May 1, 2019. Discussion period open until October 1, 2019; separate discussions must be submitted for individual papers. This paper is part of the *Journal of Bridge Engineering*, © ASCE, ISSN 1084-0702.

the steel tube and reinforced concrete core toward each other from the noncomposite to fully composite case depends on the ability of mechanisms that could transfer the forces between the steel tube and the concrete. These mechanisms could be the shear transferring bond at the concrete-to-steel tube interface or a series of attached shear transfer mechanisms at the interface.

In American codes, there are two approaches for calculating the strength of composite concrete-filled steel tube (CFST) members. One is a plastic stress distribution method (PSDM), and the other is a strain compatibility method. AISC 360 (AISC 2016) allows use of either the PSDM or strain compatibility method for calculating the strength of CFST members. ACI 318 (ACI 2014) uses a general strain compatibility method, essentially treating the CFST member as a concrete column reinforced with a structural steel tube in addition to internal reinforcement. The *AASHTO Guide Specifications for LRFD Seismic Bridge Design* (AASHTO SGS) (AASHTO 2014a) and the *Canadian Highway Bridge Design Code* (Canadian Standards Association 2006) have adopted a plastic stress method proposed by Bruneau and Marson (2004) and similar to the AISC 360 (AISC 2016) PSDM (note that the AASHTO provisions only deal with CFST without internal reinforcement). Small variations exist between the various applications of each method in different codes [described in more detail by Bruneau et al. (2018)].

The composite strength of CFSTs with internal reinforcing (i.e., RCFSTs) under cyclic loading has recently been studied by researchers (e.g., Brown et al. 2013; Moon et al. 2013; Bruneau et al. 2018). For composite RCFSTs, PSDM can be used to calculate the flexural strength by idealizing the internal steel reinforcing as a thin steel ring (Moon et al. 2012). This method was utilized by the Washington DOT *Bridge Design Manual LRFD* (WDOT 2016). The strength of a noncomposite RCFST cross section can be calculated by summation of the flexural strengths of the steel tube and the reinforced concrete core calculated individually.

Research Objectives

In essence, questions remain on how to achieve this composite action, which hampers the broader adoption of this approach. The financial savings that occur when treating the shaft as a composite member provide an incentive to answer these questions. Although it is conservative to only consider the reinforced concrete section of a drilled shaft in design when calculating its strength, it is realistic to expect that, in some conditions, a significant level of composite action (by engaging the casing) is possible. However, to be able to rely on such composite action, it must be determined under which conditions the shaft's required composite action can be achieved. For example, this may depend on the condition of the casing interior surface (clean versus coated by bentonite) before it is filled with concrete. Rabbat and Russell (1985) and Baltay and Gjelsvik (1990) measured the natural coefficient of friction at the interface of steel and concrete to be 0.57 and 0.47, respectively. Here, the results of six large-scale experimental studies performed on the cyclic flexural behavior of RCFST shafts having reinforced concrete columns at their top are presented. The flexural specimens were tested to investigate the composite action in RCFSTs with different diameters, steel tube thicknesses, shaft heights, axial loads, and steel casing-to-concrete core interface conditions. This latter issue was investigated by testing specimens with a natural steel-to-concrete bond, and specimens with reduced interface friction created by applying bentonite slurry and grease on the interior surface of the steel tube. Also, one specimen in the testing program had an alternative transition zone detail at the connection between the reinforced concrete column and the RCFST shaft to investigate a shear-head

concept developed by Bruneau et al. (2018) to transfer the column forces to the composite shaft. Finally, another specimen used a shear transfer mechanism at the top of the RCFST shaft to achieve the desired composite action when insufficient interface friction is present between the steel and concrete.

Test Specimens and Setup

A series of six cyclic large-scale flexural tests were conducted on cantilever RCFST shafts of 50.8- and 76.2-cm diameters with heights of 5.2 m (17 ft) and 7.6 m (25 ft), respectively. Each specimen consisted of a circular RCFST shaft, from which a circular reinforced concrete column (of smaller dimensions) extended at its top. The RCFST shaft was connected to a reinforced concrete foundation, which was post-tensioned to a strong floor using DYWIDAG bars (DYWIDAG-Systems International, Toughkenamon, Pennsylvania). The connection of the RCFST shaft to the foundation was designed by adapting a detail proposed by Lehman and Roeder (2012) using a circular base plate with a larger diameter than the shaft and welded to the bottom of the steel tube. Cyclic load was applied at the top of the reinforced concrete column by an actuator that was connected to a strong wall at its other end. Fig. 1 presents a three-dimensional (3D) rendering of the test specimen, with the corresponding moment diagram along its height. The test specimens were designed assuming that the reinforced concrete column (which was framed into the shaft) remained essentially elastic until the shaft reached its plastic moment capacity at its base. Although this would only be the case in practice for Type I shafts (Caltrans 2013), it was required to proceed this way here to experimentally assess the ultimate strength and ductility of the shaft at its base, such as to be able to validate design equations and assumptions. A common design method for bridge piers with single pile foundations is to protect the elements that are embedded in the soil (i.e., the pile shaft) based on capacity-based principles to ensure that the location of the plastic hinging occurs above ground level, which can be achieved, in most cases, by designing the shaft with a larger diameter than the bridge column it supports [also known as Type II shafts (Caltrans 2013)]. This makes it easy to detect possible structural damage (typically, plastic hinging or concrete spalling in the case of reinforced concrete columns or shafts) after an earthquake. However, the AASHTO SGS (AASHTO 2014a) also allows (with owner's approval) in-ground plastic hinging, recognizing that special techniques or excavation may be needed to inspect and repair following an earthquake.

The main objective of the research presented here was to investigate the composite strength of RCFST shafts. Therefore, the specimens were designed to be able to reach the ultimate strength of the enlarged shaft while protecting the column (of smaller diameter) at its top. Note that testing the shafts as Type I or Type II was not the purpose of this research, and the specimens were not categorized accordingly. Nominal material properties were used to design the reinforced column part; column and shaft lengths were selected to allow development of the expected strength of the RCFST shaft at the base. The confined compressive strength of the concrete was considered in calculating the nominal strength of the reinforced column and expected plastic moment capacity of the RCFST shaft. The confining effect of the transverse reinforcement in the reinforced concrete column was calculated according to Mander et al. (1988), whereas the confining effect of the steel tube in the shaft was calculated according to Susantha et al. (2001). The longitudinal reinforcing ratio (ρ_s) in the shaft was chosen close to 1%, because lower reinforcement ratios make it easier to design the reinforced

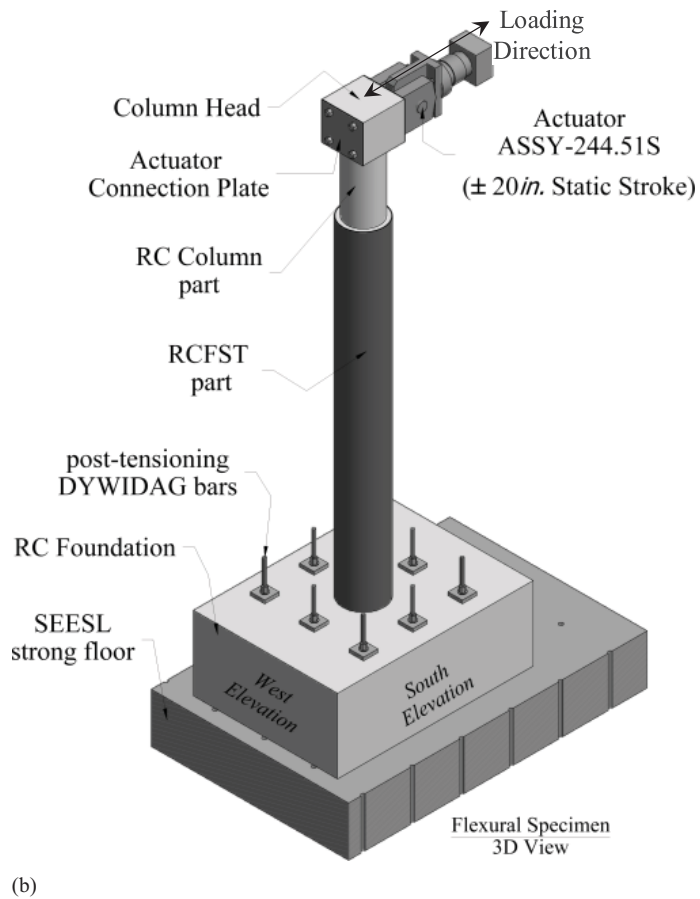
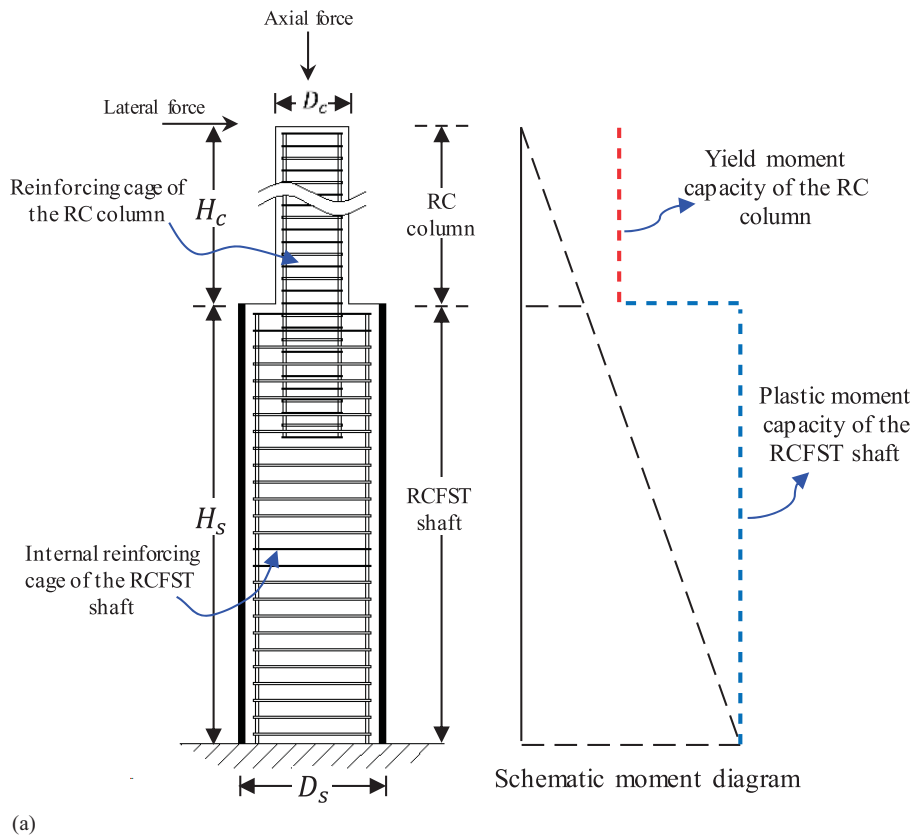


Fig. 1. (a) Design scheme of the specimens; and (b) specimens' test setup (ASSY-244.51S, MTS Systems Corporation, Eden Prairie, Minnesota). SEESL = Structural Engineering and Earthquake Simulation Laboratory.

Table 1. Properties of the test specimens

Specimen	RCFST shaft part								RC column part			
	D_s (cm)	t (cm)	$\frac{D_s}{t}$	$\frac{H_s}{D_s}$	f'_c (MPa)	f_y (MPa)	ϵ_y ($\mu\text{m}/\text{m}$)	f_u (MPa)	D_c (cm)	H_c (cm)	$\frac{H_c}{D_c}$	f'_c (specified) (MPa)
S1	50.8	0.64	80	8	34.5	317.2	1,500	379.9	40.6	101.6	2.5	27.6
S3	50.8	0.64	80	8	40.0	317.8	1,600	393.0	40.6	101.6	2.5	27.6
S4	50.8	0.64	80	8	41.4	326.8	1,400	428.2	40.6	101.6	2.5	27.6
S6R	50.8	0.64	80	8	57.2	286.1	1,400	468.8	40.6	101.6	2.5	27.6
S2R	50.8	0.64	80	8	39.3	357.8	1,700	435.1	40.6	101.6	2.5	27.6
S5	76.2	0.79	96	8	38.6	379.2	1,900	460.6	61.0	152.4	2.5	27.6

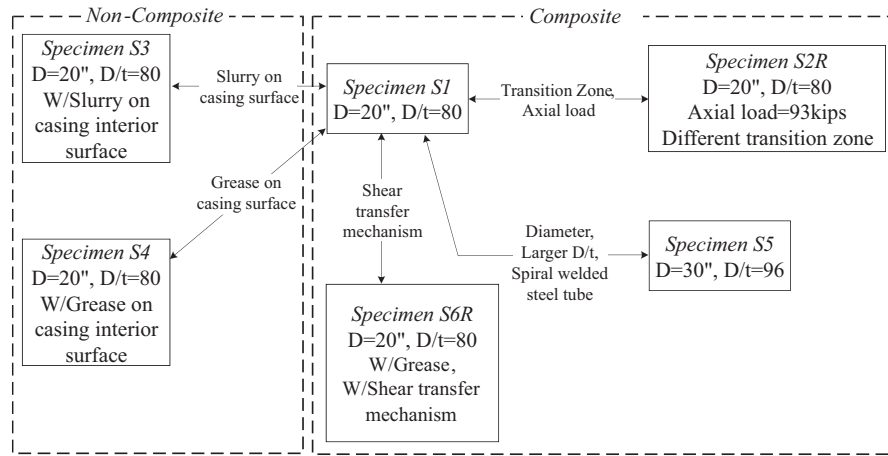


Fig. 2. Relationship of the flexural test specimens to each other.

concrete column framing into the shaft. The clear cover for the reinforced concrete core was taken to be 2.54 cm (1 in.).

The properties of the specimens are presented in Table 1, where D_s and H_s are the nominal outer diameter and the height of the shaft, respectively; t is the nominal thickness of the shaft casing; and D_c and H_c are the diameter and height of the column, respectively. All specimens were fabricated using pipes with vertical welded seams [i.e., straight-seam electric resistance welding (ERW) pipe], except for Specimen S5, which had a spiral welded pipe. ASTM (2018) Grade 2 steel with a nominal yield strength of 241.3 MPa (35 ksi) was selected for the steel tube. This material is typically approved [e.g., Washington DOT *Bridge Design Manual LRFD* (WDOT 2016)] for use as steel casing. Reinforcing cages were constructed of ASTM (2016) Grade 60 steel.

For all specimens with a 50.8-cm (20-in.) shaft diameter, the internal reinforcing cage of the RCFST part was a circular cage that consisted of 12 #5 longitudinal rebars with a #4 spiral of 10.2-cm (4-in.) pitch. A reinforcing cage of 20 #7 longitudinal rebars with #4 hoops placed at 10.2-cm (4 in.) spacings hoops was used for the reinforced concrete column. The internal reinforcing cage of the 76.2-cm (30-in.) specimen (i.e., S5) shaft was constructed of 24 #5 longitudinal rebars together with a #5 spiral of 12.7-cm (5-in.) pitch, and its reinforced concrete column was constructed of 32 #8 longitudinal rebars with #5 hoops placed at 10.2-cm (4 in.) spacings. A self-consolidating concrete (SCC) mix was used for all concrete. The length of the transition zone in the column-to-shaft connection was chosen based on the largest value of the column bar development length calculated using the equations from AASHTO BDS (AASHTO 2014b) Section 5.10.11.4.3, AASHTO SGS (AASHTO 2014a) Section 8.8.10, *Caltrans Seismic Design Criteria* (Caltrans

2013) Section 8.2.4, and Murcia-Delso (2013). The transition zone length was calculated using nominal strengths because the column part was designed to remain elastic. For all specimens, the value given by AASHTO SGS (AASHTO 2014a) governed. The distances from the top of the foundation to the top of the shaft for the 50.8-cm (20-in.) and 76.2-cm (30-in.) specimens were 406.4 cm (160 in.) and 609.6 cm (240 in.), respectively. The distances from the top of the shaft to the center of the column head were 1.02 m (40 in.) and 1.52 m (60 in.), respectively.

The test specimens and their relationship with other specimens (for comparison of experimental results to establish how various factors affect behavior) are summarized in Fig. 2. Specimen S1 was constructed and tested first as the *reference* flexural specimen against which the behavior of other specimens was to be compared. Specimen S3 was a repeat of Specimen S1 for which the inside surface of the steel tube was covered with bentonite slurry before casting the concrete as a way to simulate the effect of soil contamination in reducing the bond between the concrete and steel tube's inside surface. The bentonite slurry was poured in the steel tube with the reinforcing cage inside and then pumped out before pouring the concrete mix in it. Specimen S4 was a repeat of Specimen S3 but with a grease coating on the inside surface of the steel tube instead of slurry. The grease coating provided less friction at the interface of the concrete core and the steel tube compared to the slurry case. This was intended to provide a specimen that ideally behaved as a noncomposite for comparison purposes. Grease coating has also been used by researchers as an ultimate solution to reduce the friction at the interface of the concrete and steel tube in CFSTs (e.g., Furlong 1968; Kilpatrick and Rangan 1997; Roeder et al. 2009). Specimen S5 had a RCFST of 76.2-cm (30-in.) diameter and a $D:t$

ratio of 96 to provide information on the behavior of RCFST shafts with a higher $D:t$ ratio and to be compared to the other specimens with 50.8-cm (20-in.) diameters. A spiral welded casing was used in the RCFST to see if results would differ compared to ERW pipes. Specimen S6R was designed to investigate the effect of using shear transfer mechanisms (e.g., shear studs, welded strips) to develop composite action in a RCFST shaft in a case where no adequate friction can develop at the concrete-to-steel tube interface (which would result in a noncomposite shaft in the absence of the shear transfer mechanisms). A thick layer of grease coating was used on the interior of the steel tube of this specimen to reduce the friction. According to Bruneau et al. (2018), in the case where adequate friction cannot develop at the concrete-to-steel tube interface, composite action can be achieved by providing shear transfer mechanisms over a certain length at the top of the RCFST shaft. Four shear rings with 1.27×1.27 -cm (0.5×0.5 -in.) square cross sections and 20.3-cm (8-in.) spacing were welded at the top of the RCFST shaft of Specimen S6R, as seen in Fig. 3(a). The shear ring dimensions were designed according to Bruneau et al. (2018) to provide the required interface force for achieving composite strength of the RCFST.

Specimen S2R was similar to Specimen S1 but with two differences: (1) an external axial load [equal to approximately $0.12f'_cA_g$ of the reinforced concrete column (i.e., 413.7 kN (93 kips))] was applied at the top of Specimen S2R to investigate the flexural behavior of the reinforced concrete–RCFST shaft under axial load; and (2) the height of the reinforcing cage of the RCFST was cut shorter from its top compared to Specimen S1, leaving the top part of the shaft without reinforcing to investigate the mechanics of the load transfer between a reinforced concrete column and a CFST shaft (i.e., a RCFST with no internal reinforcing). This second difference was introduced because, based on observations from a finite-element study, full transfer of loads from the reinforced concrete column to the CFST shaft can be accomplished by a mechanism equivalent to a shear head mechanism, in the absence of shaft reinforcement, as long as the column reinforcement extends an adequate length into the shaft. Based on the finite-element analyses, the length of the column reinforcement extension into the shaft was taken as equal to summation of the diameter of the shaft (D_s) and the development length of the longitudinal bars (l_d) of the column. Fig. 3(b) presents the details of Specimen S2R. The shorter reinforcing cage in the RCFST made it possible to investigate the introduced concept of load transfer. Note that the bottom part of the shaft was reinforced to show that it could locally still develop a composite RCFST strength similar to that of Specimen S1 despite the discontinuity in reinforcement. Also note that, in Fig. 3(b), the axial load was applied by a DYWIDAG bar installed through a sleeve at the center of the cross section and post-tensioned to the axial load value. One end of this DYWIDAG bar was fixed at the top of the reinforced concrete column part of the specimen, and the other end was fixed under the strong floor.

The specimens were constructed and tested in the Structural Engineering and Earthquake Simulation Laboratory (SEESL) at the University at Buffalo (UB). Fig. 4 presents the ready-to-test view of Specimen S5 with a 76.2-cm (30-in.) diameter and test setup. The average measured material properties for each specimen are presented in Table 1. Average yield and ultimate stress for reinforcing bars were 518.5 MPa (75.2 ksi) and 666 MPa (96.6 ksi), respectively. Note that there was some noticeable scatter in the measured material properties of the steel tubes with a 50.8-cm (20 in.) diameter. A minimum number of three coupons were tested from each specimen's steel tube. Also, a minimum of three concrete cylinder samples from the shaft part of each specimen were tested on the day of testing to measure the material properties of the specimens. The

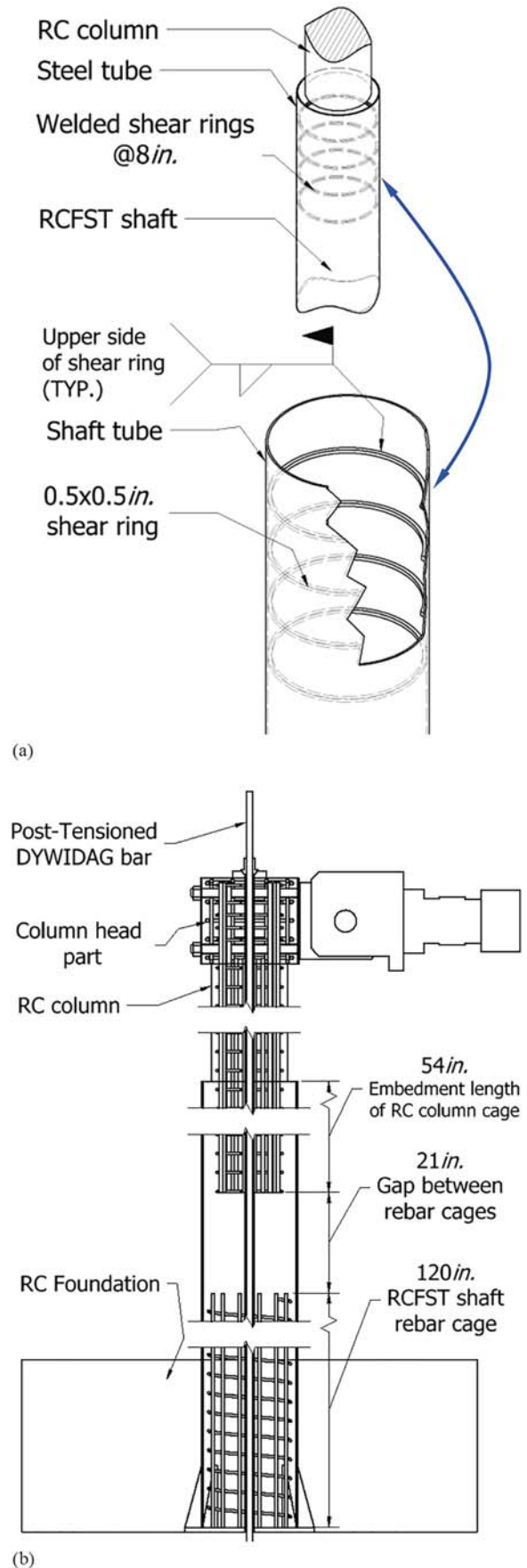


Fig. 3. (a) Specimen S6R welded shear ring details; and (b) Specimen S2R internal reinforcing details. TYP. = Typical.



Fig. 4. Global view of Specimen S5 [76.2-cm (30-in.) diameter] ready for test.

material property values presented in Table 1 are the average of all tested steel coupons and concrete cylinders for each specimen. A detailed design of the specimens, testing setup, instrumentation plans, and steel coupon and concrete cylinder test results can be found in the work by Bruneau et al. (2018).

Note that for all specimens, except for Specimen S2R, as normally done for enlarged shafts (i.e., Type II shafts), connection of the reinforced concrete column to the shaft was accomplished using noncontact splices based on McLean and Smith (1997). DOT requirements for the connection length may vary, but DOTs agree that the noncontact length provided should be based on the standard splice length, which is a function of the tension development length of longitudinal bars plus an offset distance. The development length of longitudinal bars required for column connection to an enlarged shaft was not investigated here either, because this has been addressed by others for plastic hinging above the enlarged reinforced concrete shaft [e.g., by Murcia-Delso (2013)].

Test Results and Observations

The cyclic loading protocol used for the tests consisted of four initial elastic cycles, increasing in amplitude up to first yield strength (F_y) of the specimen (i.e., force-controlled cycles). After reaching the first yield in the specimen at the end of Cycle 4, the protocol called for continued testing (in displacement-controlled cycles) by subjecting the specimen to displacement amplitudes equal to multiples of the equivalent yield displacement (Δ'_y), with two cycles applied at each displacement amplitude (i.e., at $2\Delta'_y$, $3\Delta'_y$, $4\Delta'_y$) until rupture occurred in the steel tube. The first and equivalent yield displacement amplitudes were chosen according to pushover results of nonlinear structural models of Specimens S1 and S5 analyzed in OpenSees (Mazzoni et al. 2005) for the 50.8-cm (20-in.) and 76.2-cm (30-in.) specimens, respectively. To facilitate comparison of results, all specimens with 50.8-cm (20-in.) diameter were subjected to the same cyclic displacements as applied to Specimen S1. In compliance with the cyclic displacement protocol, the displacement at the load application point was applied in cycles of progressively increasing amplitude up to the maximum stroke of the actuator [which was ± 50.8 cm (20 in.)], and after reaching that maximum cyclic amplitude [maximum cyclic amplitude reached at cycles 15 and 11 for specimens with 50.8-cm (20-in.) and 76.2-cm

(30-in.) diameters, respectively], testing continued with cycles at the same maximum displacement amplitude until failure of the specimen. The complete displacement history and key observations made during the test are presented here.

The obtained force-displacement curves for the specimens are presented in Fig. 5. The points when some of the key observations were made during the test (corresponding to the onset of visible local buckling, maximum strength, and rupture of steel tube) are marked on these curves. The displacement was measured using a string pot attached at the center of the height of the column head part shown in Fig. 1(a), and the force was measured using a load cell in the actuator.

For Specimen S1, the maximum strength of the specimen was achieved at the peak positive and negative displacements of the ninth cycle [i.e., C9P = 24.7 cm (9.74 in.) (6.1% drift) and C9N = -25.15 cm (-9.90 in.) (-6.2% drift)], with lateral loads of 202.4 kN (45.50 kips) and -202 kN (-45.39 kips), respectively (where lateral drift was calculated throughout by dividing the lateral displacement at the actuator level by the total length of the specimen from the top of the foundation to the center of the column head). Note that, for simplicity, the peak points of cycle n at peak positive and negative displacements are referenced as CnP and CnN throughout the text. For example, C9P means the maximum positive displacement attained during the ninth cycle during the test. Local buckling of the specimen started to develop during the seventh cycle of the test and was observed at the peak positive displacement of the seventh cycle (C7P). The local buckling developed approximately 5.1 cm (2 in.) above the foundation surface on both sides of the steel tube. Comparing the strain at the onset of local buckling with the yield strain (ϵ_y) of the steel tube corresponding to Specimen S1, it was observed that local buckling of the steel tube developed shortly after yielding of the steel tube on the compression side. At that point, due to the neutral axis location, the tension side of the steel tube had already yielded. This observation was consistent for all other flexural specimens. After reaching maximum flexural strength and initiation of local buckling at the bottom of the steel tube, the flexural strength of the specimen decreased upon cyclic displacements at greater amplitude. This decrease was not significant from Cycle 9 until the peak positive displacement was reached at the 15th cycle [i.e., C15P = 49.5 cm (19.49 in.) (12.2% drift)]. A first rupture of the steel tube occurred suddenly at a negative displacement of -46.4 cm (-18.28 in.) (-11.4% drift) under a lateral load of -177.5 kN (-39.9 kips) during the second half of the 15th cycle close to its peak negative displacement [i.e., C15N = -49.5 cm (-19.49 in.) (-12.2% drift)]. A second rupture on the opposite side (i.e., east side) of the steel tube occurred during the reversed displacement, at a positive displacement of 39.2 cm (15.45 in.) (9.7% drift) during the first half of the 16th cycle under a lateral force of 123.2 kN (27.7 kips). Following the second rupture, the lateral force dropped to 93.0 kN (20.9 kips) at the peak positive displacement of the 16th cycle [i.e., C16P = 49.7 cm (19.55 in.) (12.2% drift)]. At the peak negative displacement of the 16th cycle [i.e., C16N = -47.75 cm (-18.80 in.) (-11.8% drift)], the lateral load reached -77.4 kN (-17.4 kips).

Specimen S3 resisted a maximum lateral load of 170.4 kN (38.3 kips). First buckling was observed at C7P, and rupture happened at the bottom of the steel tube on the east side at the first half of the 15th cycle at a positive displacement of 46.38 cm (18.26 in.) (11.4% drift). The slippage of the concrete core with respect to the steel tube at the top of the shaft, due to reduced interface friction by the bentonite coating, was measured during the test (results are presented later in this paper). However, the amount of slippage was relatively small (particularly when

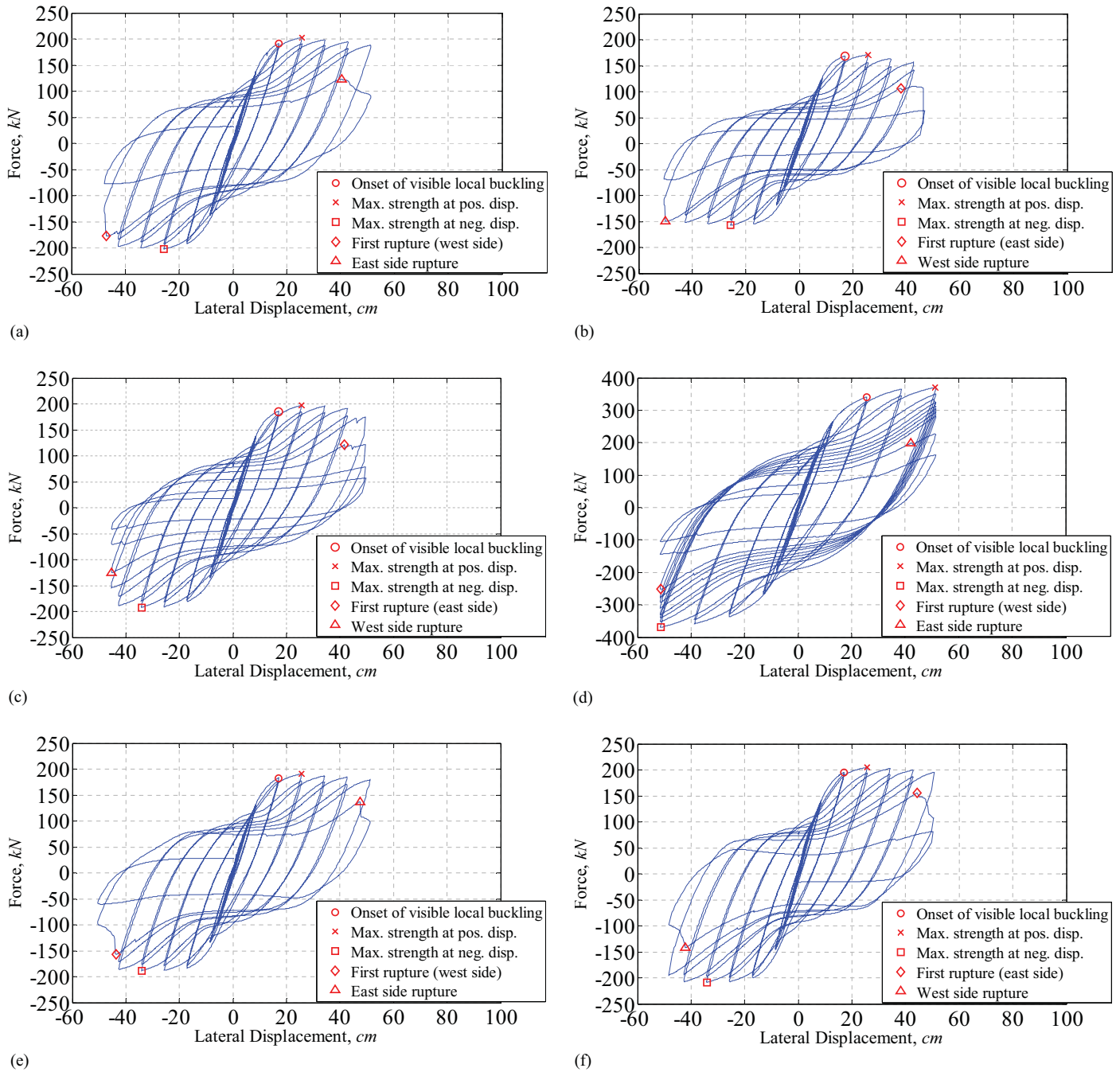


Fig. 5. Force-displacement curve measured from test of specimens: (a) S1; (b) S3; (c) S4; (d) S5; (e) S6R; and (f) S2R.

compared to that measured for Specimen S4, which had a grease coating, as is shown later). Slippage comparisons for different specimens are presented later in the text. Note that at the end of the Specimen S3 test and after rupture of the shaft tube, it was observed that the concrete at the bottom of the shaft had some moist areas, which had not been observed in other tested specimens. This was observed through the developed crack and in the concrete that fell out of the steel tube through the cracked area. The moist concrete was probably caused by the presence of the bentonite slurry in the pipe. This was also observed in other small areas on the surface of the concrete core after cutting open a part of the steel tube at the bottom of the shaft. This could have affected, to some degree, the ability of friction forces to develop at the steel tube-to-concrete interface in those areas, but not

sufficiently to prevent attainment of the plastic moment of the composite section, as is discussed later.

Specimen S4, which was built with a grease coating on the interior surface of the steel tube, resisted a maximum force of 194.4 kN (43.7 kips) at the peak positive displacement of the ninth cycle (i.e., C9P). Initiation of local buckling development was observed at the seventh cycle. Rupture at the bottom of the steel tube occurred on the east side of the tube during the first half of the 16th cycle, at a positive displacement of 41.7 cm (16.4 in.) (10.3% drift). Slippage of the concrete core with respect to the steel tube at the top of the shaft part was visually observed from the 12th cycle. Significantly more slippage between the steel casing and the concrete developed than what was observed in Specimen S3 (with bentonite coating). The measured slippages are presented later.

Specimen S5 resisted a maximum lateral load of 369.6 kN (83.1 kips) at the peak positive displacement of the 11th cycle. Local buckling was visually observed at the seventh cycle. The actuator's maximum stroke of 50.8 cm (20 in.) was reached at the 11th cycle. Therefore, testing continued with cycles of the same displacement amplitude until failure of the specimen. Maximum flexural strength of the specimen reduced progressively after the 11th cycle, and failure occurred by rupture of the steel tube at the bottom of the RCFST. First rupture occurred just prior to reaching the maximum negative displacement during the 18th cycle (i.e., C18N) at a negative displacement of -51.3 cm (-20.2 in.) (8.4% drift) on the west side of the steel tube. Rupture on the east side occurred during the following displacement half-cycle, toward the maximum positive displacement of the 19th cycle, at a displacement of 42.2 cm (16.6 in.) (6.9% drift). Testing continued for an additional cycle, after which the crack had propagated to a length of 76.2 cm (30 in.) on the west side and 57.15 cm (22.5 in.) on the east side of the tube.

The objective of testing Specimen S6R was to investigate the possibility of developing the full composite strength of the RCFST shaft by means of a shear transfer mechanism (i.e., the rings) in the absence of adequate friction at the concrete-to-steel tube interface. Specimen S6R was constructed with a thick coating of grease on the interior surface of the steel tube and with shear rings welded at the top of the steel tube. This specimen resisted a maximum lateral load of 190.4 kN (42.8 kips) at the peak positive displacement of the ninth cycle (i.e., C9P). Initiation of local buckling was observed at the seventh cycle, and rupture at the bottom of the steel tube occurred on the west side of the tube during the second half of the 15th cycle at a negative displacement of -43.7 cm (-17.2 in.) (-10.8% drift). No visible slippage at the interface was observed during the test.

Specimen S2R, which was constructed and tested with a different transition zone and under axial load, resisted a maximum lateral load of 204.6 kN (46.0 kips) at the positive peak displacement of the ninth cycle (C9P) and -207.0 kN (-46.54 kips) at the negative peak displacement of the 11th cycle (C11N). The development of local buckling at the bottom of the steel tube was visually observed at the peak displacement of the seventh cycle [C7P = 17.1 cm (6.73 in.) (4.2% drift)]. At this point, specimen resistance was 194.6 kN (43.74 kips), which was 95% of the maximum lateral load resisted by the specimen. Comparing the experimentally obtained strains at the buckling zone of the steel tube with its yield strain shows that the buckling developed after yielding. First rupture of the steel tube occurred on the east side of the steel tube during the first half of the 16th cycle at a positive displacement of 44.45 cm (17.5 in.) (10.9% drift) under a lateral load of 155.7 kN (35 kips). Upon load reversal, the west side of the steel tube ruptured as the displacement reached -42.16 cm (-16.6 in.) (-10.4% drift) under a lateral load of 138.8 kN (-31.2 kips). It was observed that the steel tube started to tear due to accumulative plastic strain at the points of highest curvature along the buckled zone. It appeared that when cracking initiated locally, it was not through the entire thickness of the tube, but this could not be verified by measurements. This might have created a progressive reduction in the effective thickness of the steel tube before through-thickness fracture eventually developed in the steel tube.

As discussed before, the axial load on Specimen S2R was applied by means of a DYWIDAG bar that was placed along the specimen and pretensioned to approximately 11% of the axial capacity (squash load) of the reinforced concrete column part. The axial load applied on Specimen S2R and its variation during the cycles is presented in Figs. 6(a and b) with respect to loading cycles and lateral displacements at the top of the specimen, respectively.

As seen in Fig. 6(b), the axial load on the specimen increased as the lateral displacement at the top of the specimen increased. This is attributed to elongation of the pretensioned DYWIDAG bar that occurred in each cycle as it was placed at the center of the cross section, where tension developed as the position of the neutral axis shifted away from the center of the cross section. The progressive increase in axial force throughout the test program [as seen in Fig. 6(a)] was found to be a consequence of the increase in length of the specimen during the inelastic cycles. This increase in length of the specimen was observed (i.e., replicated) in the finite-element analysis of Specimen S2R (Bruneau et al. 2018). The increase in length of the specimen was not measured during the test. As seen in Fig. 6, the values of the axial load varied between 411.9 kN (92.6 kips) and 636.1 kN (143.0 kips) (i.e., ranging between 12 and 18% of the axial capacity of the reinforced concrete column).

It was also observed in Specimen S2R that even in the absence of internal reinforcing over the middle part of the RCFST shaft, forces were able to transfer from the reinforced concrete column to the shaft, and the shaft was still able to develop its theoretical plastic moment. This suggests that the load-transferring mechanism that was described could be used as an alternative transition zone design.

Fig. 7 presents the development of local buckling at the lower part of the steel tube of Specimen S2R (as a representative of local buckling development of the specimens) for different peak displacements. Figs. 8(a and b) present the ruptured steel tube on the east and west sides of the steel tube, respectively, for Specimen S1

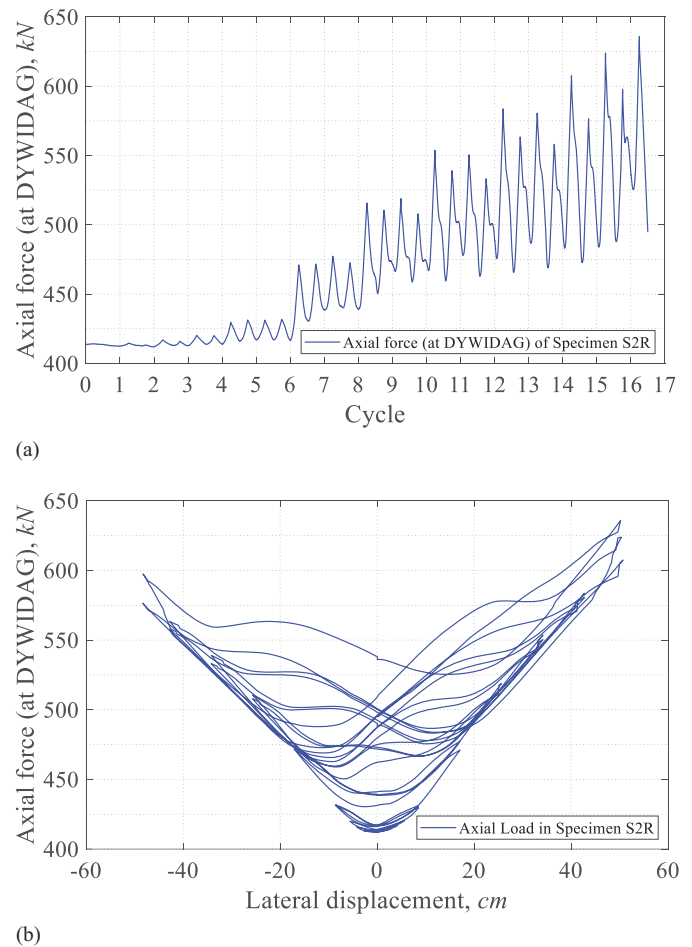


Fig. 6. Specimen S2R's applied axial load variations versus (a) cycles; and (b) lateral displacement.

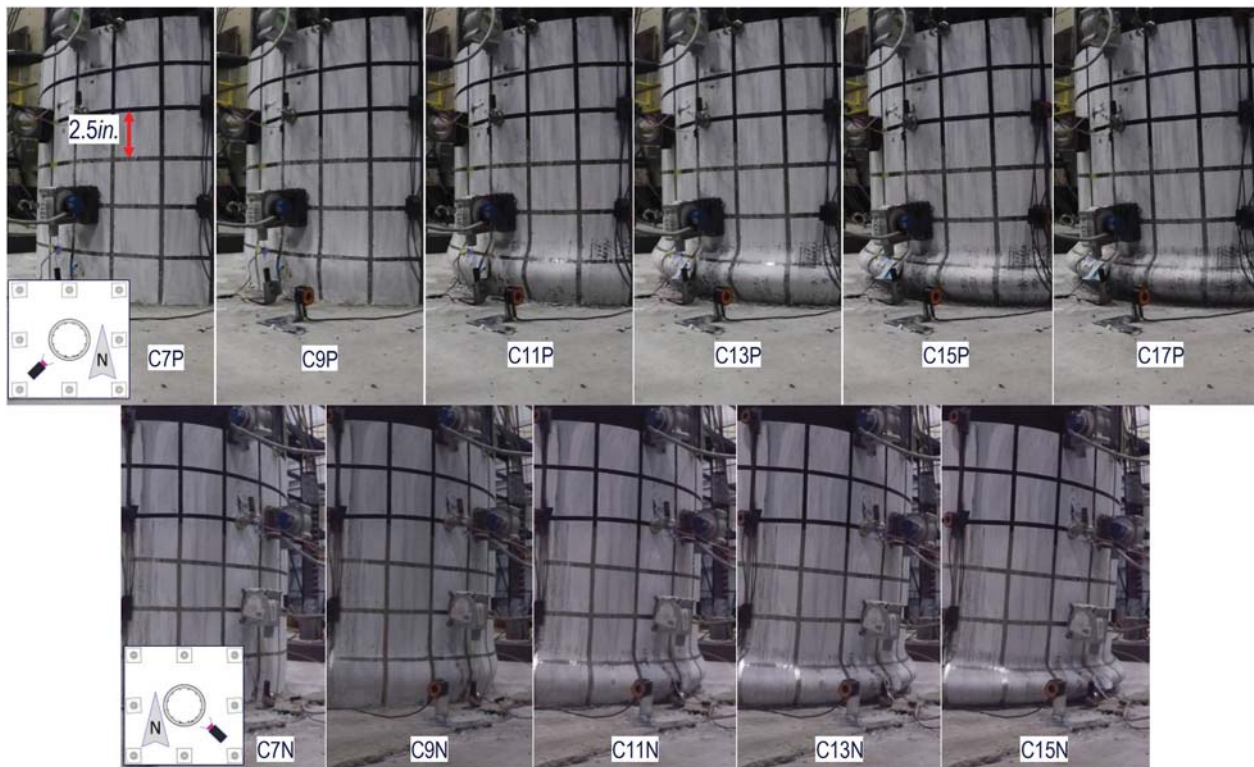


Fig. 7. Development of tube local buckling at lower part of Specimen S2R at different peak displacements.

as a representative example of steel tube rupture in the tested specimens. More details regarding the deformed shapes of the specimens and the comparison of their hysteresis curves with each other can be found in the work by Bruneau et al. (2018).

The average slippages at the interface of the steel tube and the concrete core at the top of the shaft, as measured using Krypton (SEESL 2018) light-emitting diodes (LEDs) on each tested specimen, are compared in Fig. 9. Generally, the slippages were insignificant, typically less than 1.27 mm (0.05 in.), except for Specimen S4 (i.e., the specimen with grease coating on the interior surface of the steel tube), which was significantly higher than for all other specimens. The maximum slippage for Specimen S4 was more than a third of inch [9.1 mm (0.36 in.)]. As presented in Fig. 9, the slippage for Specimen S1 was within 0.12 mm (0.0046 in.) (78 times less than for S4) and did not increase at greater lateral displacements. For Specimen S2R, the measured slippages were within 0.10 mm (0.0041 in.). The measured slippage for Specimen S3 increased as the lateral displacement increased. However, as seen in Fig. 9, the measured slippage was still significantly less compared to the slippage experienced by Specimen S4. The maximum measured slippage for Specimen S3 was 0.43 mm (0.017 in.), which was 3.6 times more than the maximum measured slippage for Specimen S1 but still approximately 20 times less than that for Specimen S4. For the larger-diameter specimen (Specimen S5), the slippages were within 0.21 mm (0.0081 in.), which was 1.77 times the maximum slippage for Specimen S1. The slippages for Specimen S6R, which had grease coating on the interior surface of its steel tube and shear rings at the top of the RCFST shaft, increased with lateral displacement. But contrary to Specimen S4 (i.e., the other specimen with grease coating but without shear rings), the maximum slippage was only 0.84 mm (0.033 in.) at the maximum lateral displacement, which was 10.6 times less than Specimen S4. This indicates that the shear rings at the top of the steel tube of the RCFST shaft were able to prevent slippage.

Beyond the measurements from the instrumentation, slippage between the steel tube and the concrete core was *visually* observable at the top of the RCFST shaft for Specimen S4 only; for all other specimens, no visible slippage was observed. Figs. 10(a and b) present the condition of the top of the RCFST shaft part for Specimen S4, for which the slippage was visually observed, and for Specimen S3, for which there was nonvisible (but measured) slippage, respectively.

Comparison of Specimens' Strengths

A comparison of the experimentally obtained strength of flexural specimens with each other and with their corresponding analytically calculated composite and noncomposite section strengths is presented in Figs. 11–13 and Table 2. To compare the flexural specimen results with each other, the experimentally obtained strength for each flexural specimen was normalized to its analytical strength, and normalized values were compared to each other. The analytical strengths were calculated using the PSDM, considering each specimen's test condition (such as applied axial load and composite or noncomposite behavior) and the variation of each specimen's measured material properties. To account for these variations and their effects, the analytical strength was calculated using all possible combinations of each tested steel coupon and concrete cylinder for each specimen. This was done to include the possible effects of variations in the material. The confining effects of the steel tube were considered in the PSDM calculations using the proposed model by Susantha et al. (2001).

For analytical strength calculations of Specimen S2R, which was axially post-tensioned to an axial value of 413.7 kN (93 kips) before testing but for which this axial load increased up to 636.1 kN (143 kips) during the test, this variation in axial load was considered

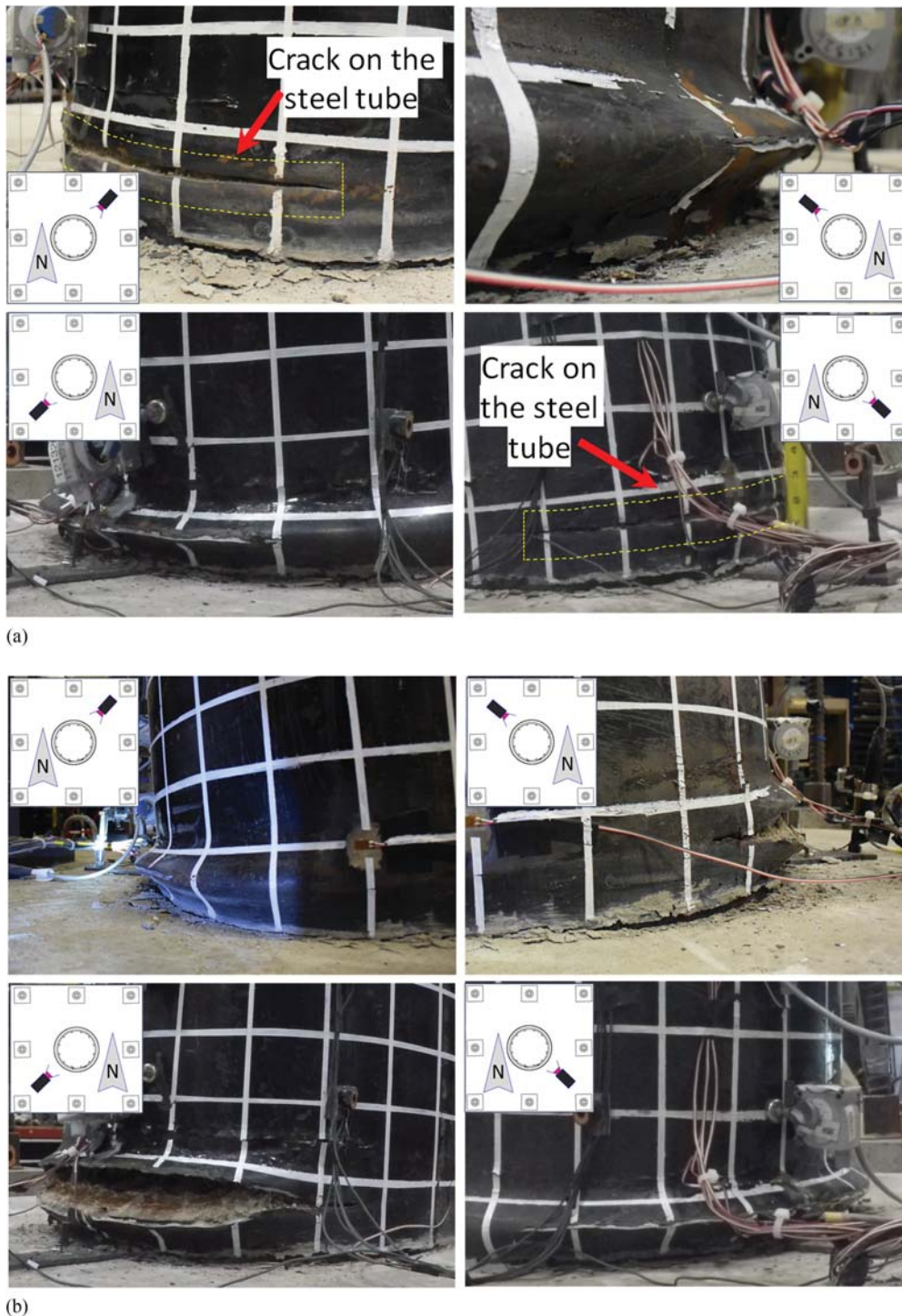


Fig. 8. Lower part of Specimen S1 at (a) C16P; and (b) C16N.

in calculating the dispersion of the strengths. This means that two levels of axial load were also considered in the possible combinations to calculate the analytical strengths for this specimen. The variation of analytical strength considering the average of the material properties but using these two axial load levels was less than 2.5%. Also for this case, in addition to the PSDM calculations (which considered material strength but no second-order effects), a simple discrete-finite-element model of the specimen was developed in OpenSees (Mazzoni et al. 2005) to consider the possible P - Δ effects and variations of axial load due to lateral deformations of the

specimen. The developed finite-element model was a fiber model that made it possible to capture the variations that occurred during the test in the pretension load in the DYWIDAG bar used to apply axial load on the specimen.

Fig. 11(a) presents the dispersion of the calculated strengths for each flexural specimen using PSDM and various ways to account for the variation in material properties obtained from sample to sample (because there was some noticeable scatter in material properties). In Fig. 11, the analytical composite strength (F) was calculated for all combinations of the uniaxial yield strength of the tube

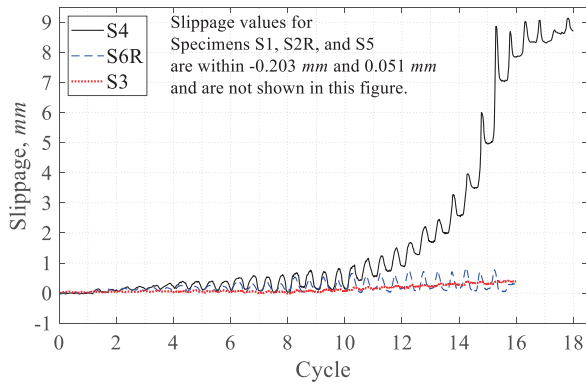
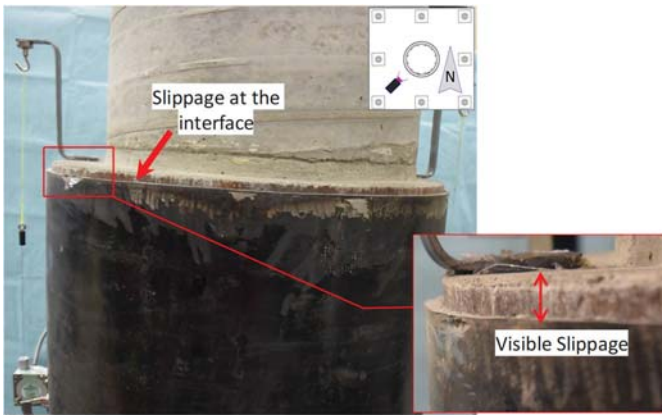


Fig. 9. Comparison of measured slippage at the interface of steel tube and concrete core of specimens measured by Krypton LEDs.



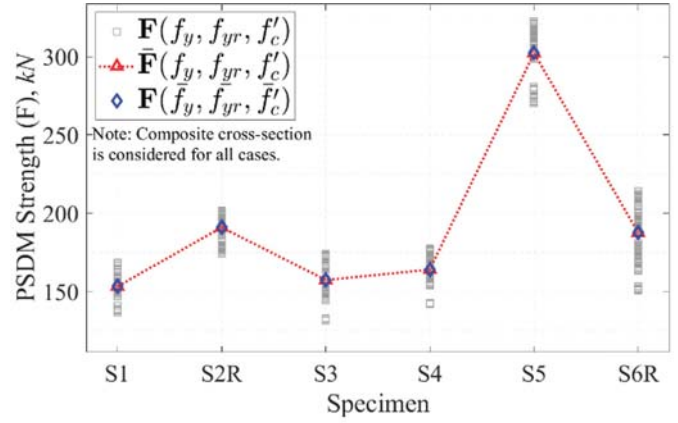
(a)



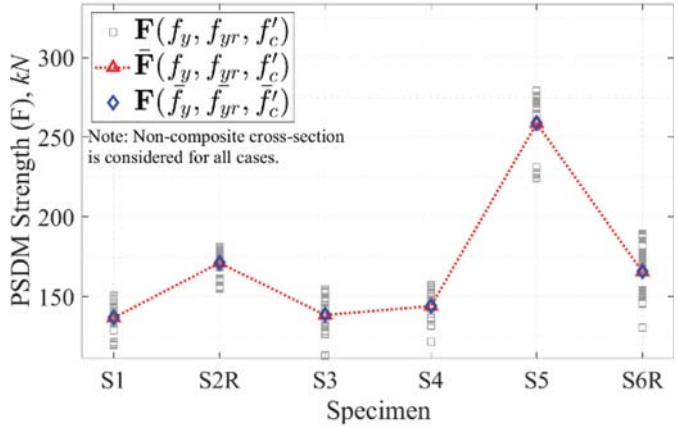
(b)

Fig. 10. (a) Visible slippage at top of the shaft part of Specimen S4 at the end of the test; and (b) top of the shaft part of Specimen S3.

(f_y) and RCFST shaft longitudinal bars (f_{yr}) obtained from test coupons and the uniaxial compressive strength of the RCFST shaft concrete (f'_c) obtained from cylinders for each specimen. These values are presented as gray circles in Fig. 11. The average values of the strength computed using all of these combinations [$\bar{F}(f_y, f_{yr}, f'_c)$] and the strength that was calculated using average material properties [i.e., $F(\bar{f}_y, \bar{f}_{yr}, \bar{f}'_c)$] are presented as well. Note that the values of $\bar{F}(f_y, f_{yr}, f'_c)$ and $F(\bar{f}_y, \bar{f}_{yr}, \bar{f}'_c)$ were close to each



(a)



(b)

Fig. 11. Dispersion of PSDM analytical strengths considering (a) composite cross section; and (b) noncomposite cross section.

other (averages of PSDM strengths and the PSDM strength of the average of the material properties were not identical because the location of the plastic neutral axis was different for each combination of material strengths, and the average of these plastic neutral axis locations will be different than the plastic neutral axis from the average material properties). The same calculations were done considering noncomposite behavior of the cross section for all flexural specimens, and results are presented in Fig. 11(b). The noncomposite strength was simply calculated using PSDM for the steel tube and reinforced concrete separately and then adding those two values together. The normalized strengths were calculated per Eqs. (1) and (2)

$$\hat{F}_C = \frac{F_{\text{exp}}}{F_{C,\text{PSDM}}} \quad (1)$$

$$\hat{F}_{NC} = \frac{F_{\text{exp}}}{F_{NC,\text{PSDM}}} \quad (2)$$

where F_{exp} = experimentally obtained strength of the flexural specimen; $F_{C,\text{PSDM}}$ = PSDM strength using average material properties [$F(\bar{f}_y, \bar{f}_{yr}, \bar{f}'_c)$] for the composite cross section; and $F_{NC,\text{PSDM}}$ = PSDM strength using average material properties [$F(\bar{f}_y, \bar{f}_{yr}, \bar{f}'_c)$] for the noncomposite cross section. The calculated normalized strengths and their mean for each flexural specimen are presented in Fig. 12. All normalized mean strengths were greater than 1, which

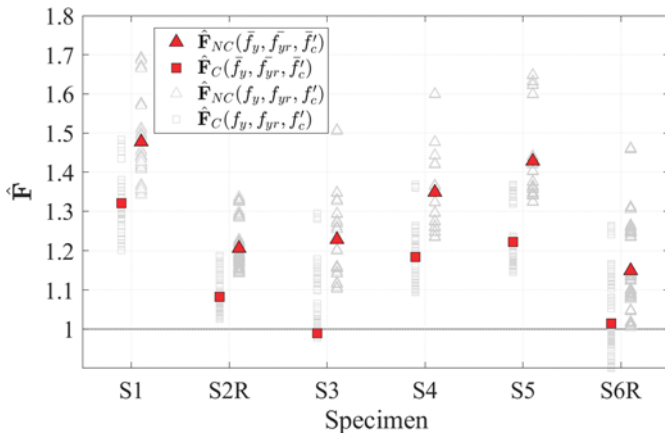


Fig. 12. Normalized specimens' strengths.

means that the experimentally obtained values were greater than the analytically predicted strengths using PSDM.

Table 2 presents a summary of the experimentally obtained and the analytically calculated mean strengths for each flexural specimen. For Specimen S2R, which was axially post-tensioned to an axial value of 413.7 kN (93 kips) before testing, the analytical strengths are presented for cases with and without the axial load in the fifth row of Table 2. As seen in Table 2, the experimental strengths for all specimens were more than the composite analytical strengths, which suggests that the required composite action was achieved for these specimens. For Specimen S1, the strengths of the specimen were 32% and 48% higher than the analytically calculated composite and noncomposite strengths (i.e., \hat{F}_C and \hat{F}_{NC} , respectively, in Table 2), respectively.

For the axially loaded flexural specimen (i.e., Specimen S2R), PSDM results show that the presence of axial load increased the analytical strengths by 6.7% and 8.8% for the composite and noncomposite cases, respectively. The normalized composite strength of Specimen S2R with axial load (having $\hat{F}_{C,S2R} = 1.10$) compared to the normalized composite strength of Specimen S1 (having $\hat{F}_{C,S1} = 1.32$) indicates that the axial load did not increase the composite strength (i.e., $\hat{F}_{C,S2R} < \hat{F}_{C,S1}$).

Specimens S3 and S4, which had bentonite slurry and grease at their steel-to-concrete interface, respectively, had lower normalized strengths than Specimen S1. However, both showed greater strengths than the analytically calculated strength for the noncomposite case. For Specimen S4, slippage at the interface of the steel tube and concrete core was observed, which is discussed later. For Specimen S5, which had a larger diameter and $D:t$ ratio, the normalized strengths were 7.6% and 3.4% less for composite and noncomposite cross sections, respectively, compared to corresponding values for Specimen S1. The normalized strengths for Specimen S6R were also less than the corresponding values for Specimen S1. Specimen S6R had a grease coating on the interior surface of the steel tube, and shear rings were welded at the top of the RCFST shaft part to achieve composite behavior at the RCFST shaft cross section. The normalized strengths were 22.7 and 22.3% less than Specimen S1 composite and noncomposite cases, respectively. However, as is seen in Table 2, the mean values were more than 1, which shows that the experimentally obtained strength was more than the analytically calculated cross-section strengths. The resistance contribution ratios of steel tube and reinforced concrete core to the total composite strength are also presented in Table 2. The envelopes of

Table 2. Experimentally obtained and analytically calculated strength comparison

Specimen	Specimen strength [F_{exp} (kN)] (experimental)	Composite strength [$F_{C,PSDM}$ (kN)] (PSDM)	Noncomposite strength [$F_{NC,PSDM}$ (kN)] (PSDM)	Normalized composite strength ($\hat{F}_C = \frac{F_{exp}}{F_{C,PSDM}}$)	Normalized noncomposite strength ($\hat{F}_{NC} = \frac{F_{exp}}{F_{NC,PSDM}}$)	Steel tube resistance ratio	RC core resistance ratio
S1	202.4	153.5	137.0	1.32	1.48	0.57	0.43
S3	170.4	157.5	138.8	1.10	1.23	0.53	0.47
S4	194.4	164.1	144.1	1.19	1.35	0.54	0.46
S6R	190.4	187.7	165.5	1.02	1.15	0.60	0.40
S2R	206.8	178.8 (no axial)	157.5 (no axial)	1.16	1.31	0.58	0.42
		190.8 (with axial)	171.3 (with axial)	1.10	1.21	0.56	0.44
S5	369.6	302.5	258.9	1.22	1.43	0.44	0.56

the maximum forces reached at each amplitude of lateral displacement seen in Fig. 5 (i.e., the backbone of the force-displacement curves) were normalized to the calculated average analytical strengths and compared to Specimen S1 in Fig. 13. Results were generally similar for all specimens.

Conclusions

Six large-scale RCFST shafts with reinforced concrete columns at their top were subjected to cyclic flexural loading. The observations from the tests were as follows:

- Results from Specimen S1 (which was the reference specimen for comparison with the other flexural specimens) showed that the existing friction coefficient that naturally develops at the interface of the steel tube and the concrete core of the shaft was adequate to develop a composite strength exceeding the theoretical plastic strength calculated by the PSDM. Indeed, all tested flexural specimens exceeded the PSDM strengths by an average of 16%.
- Testing of Specimen S2R demonstrated that there exists a transition zone at the top of the shaft that makes it possible

to transfer the forces developed by the reinforced concrete column attached at the top of the shaft, even in the absence of reinforcement in the shaft (except for the column bars extending into the shaft by their required development length). In fact, with reinforcement introduced only in the bottom part of the shaft 53.3 cm (21 in.) below the point where the column reinforcement was discontinued, the RCFST shaft theoretical plastic moment could be developed at the bottom of the shaft. Also, no significant increase in the strength of the RCFST shaft due to axial load was observed in the testing of Specimen S2R.

- A *pure* condition of noncomposite action did not occur when the inside of the steel shaft was coated using either bentonite slurry or grease, as were the cases in Specimens S3 and S4, respectively. In fact, both specimens exceeded the composite and noncomposite PSDM strengths by an average of 15% and 29%, respectively. In Specimen S3, a moist area on the outside surface of the concrete core, presumably due to the bentonite slurry, was observed at the bottom of the shaft, and it appears that the strength of the RCFST shaft was somewhat reduced as a consequence (even though it still exceeded the plastic strength). In Specimen S4, slippage occurred during testing

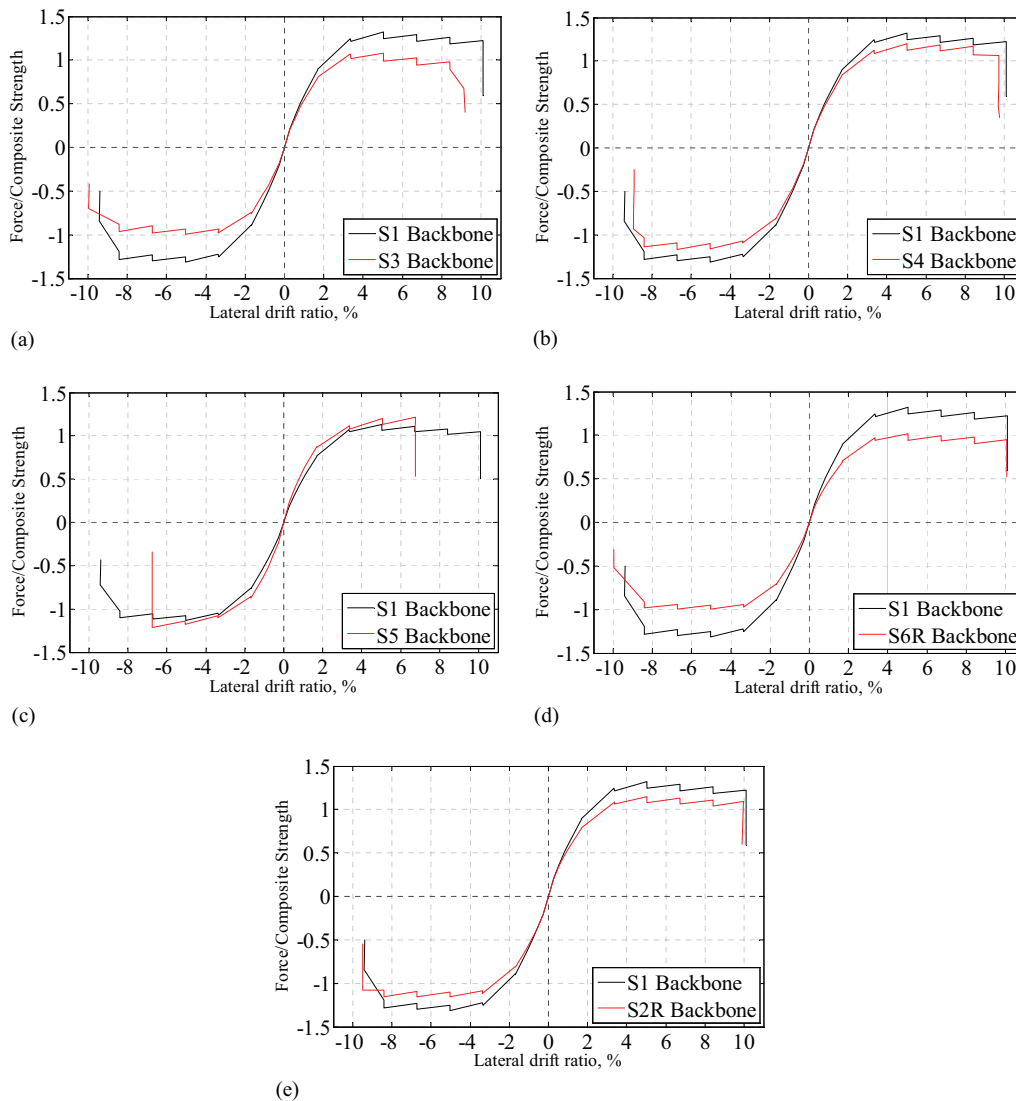


Fig. 13. Comparison of normalized backbone curves for Specimens S1 and (a) S3; (b) S4; (c) S5; (d) S6R; and (e) S2R.

only at the larger displacements, which was considered to be an indication of noncomposite shaft behavior at these larger cycles. No such significant slippage was recorded for Specimen S3.

- Comparison of the test results for Specimens S5 and S1 showed that the change in the diameter of the shaft (and an increase in the $D:t$ ratio from 80 to 96) did not affect the ability of the RCFST to achieve composite behavior when only relying on the friction that naturally developed between the steel tube and concrete. Furthermore, Specimen S5 was constructed with a spirally welded steel tube and was still able to develop its full plastic moment and an inelastic cyclic response comparable to that of the other specimens.
- The investigation of the amount of composite action for RCFSTs, even with contaminated interiors of steel tubes, showed substantial composite behavior even when no additional steps were taken to transfer the internal shear at the interface of concrete and the steel tube.
- Specimen S6R, with welded shear rings at the top end of the shaft, designed based on the *transferred internal axial load* demand calculated using the proposed equation by Bruneau et al. (2018), was able to develop the composite action at the RCFST shaft. The behavior of RCFST shafts embedded in soil, which was investigated in a separate study, together with analyses to determine locations of the shear rings that are effective in that condition will be the subject of a future study. In addition, future research is needed to provide more test data on the new transition zone concept that was identified in Specimen S2R.

Acknowledgments

This work was sponsored by AASHTO in cooperation with the FHWA and was conducted in the National Cooperative Highway Research Program (NCHRP), which is administrated by the Transportation Research Board (TRB) of the National Academies of Sciences, Engineering, and Medicine, under the research project NCHRP 12-93. The authors thank the NCHRP 12-93 Program Officer and the other members of the project's advisory panel. However, the opinions, findings, conclusions, and recommendations presented in this report are those of the authors and do not necessarily reflect acceptance by or the views of the National Academy, the TRB, FHWA, or AASHTO.

References

- AASHTO. 2014a. *AASHTO guide specifications for LRFD seismic bridge design*. 2nd ed., with 2015 interim revisions. Washington, DC: AASHTO.
- AASHTO. 2014b. *AASHTO LRFD bridge design specifications, customary U.S. units*. 7th ed., with 2015 Interim Revisions. Washington, DC: AASHTO.
- ACI (American Concrete Institute). 2014. *Building code requirements for structural concrete: (ACI 318-14) and commentary (ACI 318R-14)*. ACI 318-14. Farmington Hills, MI: ACI.
- AISC (American Institute of Steel Construction). 2016. *Specification for structural steel buildings*. AISC 360-16. Chicago: AISC.
- ASTM. 2016. *Standard specification for deformed and plain low-alloy steel bars for concrete reinforcement*. A706/A706M-16. West Conshohocken, PA: ASTM.
- ASTM. 2018. *Standard specification for welded and seamless steel pipe piles*. A252-10. West Conshohocken, PA: ASTM.

- Baltay, P., and A. Gjelsvik. 1990. "Coefficient of friction for steel on concrete at high normal stress." *J. Mater. Civ. Eng.* 2 (1): 46–49. [https://doi.org/10.1061/\(ASCE\)0899-1561\(1990\)2:1\(46\)](https://doi.org/10.1061/(ASCE)0899-1561(1990)2:1(46)).
- Brown, D. A., J. P. Turner, and R. J. Castelli. 2010. *Drilled shafts: Construction procedures and LRFD design methods*. Report No. FHWA-NHI-10-016. Washington, DC: Federal Highway Administration.
- Brown, N. K., M. Kowalsky, and J. Nau. 2013. *Strain limits for concrete filled steel tubes in AASHTO seismic provisions*. Fairbanks, AK: Alaska Dept. of Transportation and Public Facilities.
- Bruneau, M., H. Kenarangi, and T. P. Murphy. 2018. *NCHRP research Rep. 872 contribution of steel casing to single shaft foundation structural resistance*. NCHRP Research Rep. 872. Washington, DC: Transportation Research Board.
- Bruneau, M., and J. Marson. 2004. "Seismic design of concrete-filled circular steel bridge piers." *J. Bridge Eng.* 9 (1): 24–34. [https://doi.org/10.1061/\(ASCE\)1084-0702\(2004\)9:1\(24\)](https://doi.org/10.1061/(ASCE)1084-0702(2004)9:1(24)).
- Caltrans. 2010. *Caltrans seismic design criteria version 1.6*. Sacramento, CA: California Dept. of Transportation.
- Caltrans. 2013. *Caltrans seismic design criteria version 1.7*. Sacramento, CA: California Dept. of Transportation.
- Canadian Standards Association. 2006. *Canadian highway bridge design code*. Mississauga, ON, Canada: Canadian Standards Association.
- FDOT (Florida Dept. of Transportation). 2000. "Soils and foundation handbook." Accessed March 1, 2014. <http://www.fdot.gov/structures/Manuals/sfh2000.pdf>.
- Furlong, R. W. 1968. "Design of steel-encased concrete beam-columns." *J. Struct. Div.* 94 (1): 267–282.
- KDOT (Kansas Dept. of Transportation). 2013. *Bridge LRFD design manual*. Vol. III. Topeka, KS: KDOT.
- Kilpatrick, A. E., and B. V. Rangan. 1997. *Deformation-control analysis of composite concrete columns*. Perth, Australia: School of Civil Engineering, Curtin Univ. of Technology.
- Lehman, D. E., and C. W. Roeder. 2012. "Foundation connections for circular concrete-filled tubes." *J. Constr. Steel Res.* 78: 212–225. <https://doi.org/10.1016/j.jcsr.2012.07.001>.
- Mander, J. B., M. J. N. Priestley, and R. Park. 1988. "Theoretical stress-strain model for confined concrete." *J. Struct. Eng.* 114 (8): 1804–1826. [https://doi.org/10.1061/\(ASCE\)0733-9445\(1988\)114:8\(1804\)](https://doi.org/10.1061/(ASCE)0733-9445(1988)114:8(1804)).
- Mazzoni, S., F. McKenna, M. H. Scott, and G. L. Fenves. 2005. *OpenSees command language manual*. Berkeley, CA: Pacific Earthquake Engineering Research (PEER) Center.
- McLean, D., and C. Smith. 1997. *Noncontact lap splices in bridge Column-Shaft connections*. Olympia, WA: Washington State Dept. of Transportation.
- Missouri Dept. of Transportation. 2011. *Engineering policy guidelines for design of drilled shafts*. Final Rep. for Project TRyy0922, Rep. cmr12003. Jefferson City, MO: Missouri Dept. of Transportation.
- Moon, J., D. E. Lehman, C. W. Roeder, and H. E. Lee. 2013. "Strength of circular concrete-filled tubes with and without internal reinforcement under combined loading." *J. Struct. Eng.* 139 (12): 04013012. [https://doi.org/10.1061/\(ASCE\)ST.1943-541X.0000788](https://doi.org/10.1061/(ASCE)ST.1943-541X.0000788).
- Moon, J., C. W. Roeder, D. E. Lehman, and H.-E. Lee. 2012. "Analytical modeling of bending of circular concrete-filled steel tubes." *Eng. Struct.* 42: 349–361. <https://doi.org/10.1016/j.engstruct.2012.04.028>.
- Murcia-Delso, J. 2013. "Bond-slip behavior and development of bridge column longitudinal reinforcing bars in enlarged pile shafts." Ph.D. thesis, Univ. of California San Diego.
- NDOT (Nevada Dept. of Transportation). 2008. *Structures manual*. Carson City, NV: NDOT.
- Oregon Dept. of Transportation. 2013. *Bridge design and drafting manual*. Salem, OR: Oregon Dept. of Transportation.
- Rabbat, B., and H. Russell. 1985. "Friction coefficient of steel on concrete or grout." *J. Struct. Eng.* 111 (3): 505–515. [https://doi.org/10.1061/\(ASCE\)0733-9445\(1985\)111:3\(505\)](https://doi.org/10.1061/(ASCE)0733-9445(1985)111:3(505)).
- Roeder, C. W., D. E. Lehman, and R. Thody. 2009. "Composite action in CFT components and connections." *Eng. J.* 46 (4): 229–242.

SCDOT (South Carolina Dept. of Transportation). 2008. *Seismic design specifications for highway bridges*. Columbia, SC: SCDOT.

SEESL (Univ. at Buffalo Structural and Earthquake Engineering Simulation Laboratory). 2018. "SEESL lab manual." Accessed August 8, 2018. <http://nees.buffalo.edu/docs/labmanual/SEESLLabManual.pdf>.

Susantha, K., H. Ge, and T. Usami. 2001. "Uniaxial stress–strain relationship of concrete confined by various shaped steel tubes." *Eng. Struct.* 23 (10): 1331–1347. [https://doi.org/10.1016/S0141-0296\(01\)00020-7](https://doi.org/10.1016/S0141-0296(01)00020-7).

WDOT (Washington Dept. of Transportation). 2016. *Bridge design manual LRFD*. Olympia, WA: WDOT.